Nonisothermal Crystallization Kinetics Study of LDPE/MWCNT Nanocomposites: Effect of Aspect Ratio and Surface Modification

Sarfraz H. Abbasi, Ibnelwaleed A. Hussein, M. Anwar Parvez

Department of Chemical Engineering and Center of Research Excellence in Petroleum Refining & Petrochemicals, KFUPM, Dhahran 31261, Saudi Arabia

Received 23 January 2010; accepted 29 March 2010
DOI 10.1002/app.32536
Published online 21 July 2010 in Wiley Online Library (wileyonlinelibrary.com).

ABSTRACT: In this article, the effect of aspect ratio and chemical modification of multiwall carbon nanotubes (MWCNT) on the nonisothermal crystallization kinetics of LDPE/MWCNT nanocomposites was studied. Nine different samples were prepared using different MWCNT to study both effects. The cooling rate (R) was varied in the range 2–10°C/min. In this article, the effect of CNT loading, surface modification, and aspect ratio were studied. For the same MWCNT concentration, aspect ratio and —COOH modification had weak influence on both the peak crystallization temperature and the crystallization onset temperature. However, the crystallization onset temperature was significantly affected by the amount of MWCNT. The rate parameters in the modified Avrami method and Mo method [$F(T)$] of analyses show a very good fit of data. The Vyazovkin and Sbirrazzuoli method of analysis, which is based on Hoffman–Lauritzen theory for secondary crystallization, was also used. Temperature dependency of activation energy was obtained for 30–75% relative crystallinity of the produced nanocomposites. Activation energy based on calculations of Hoffman-Lauritzen theory showed a decrease with the increase in the concentration of MWCNT and crystallization temperature. A proposed model of the form $E = a \exp(-bXT)$ which relates the activation energy, E, to relative crystallinity, X, and crystallization temperature, T, was able to fit the whole set of data. Incorporation of MWCNT in nanocomposites lowers the activation energy; hence enhances the initial crystallization process as suggested by the different methods of data analyses. J Appl Polym Sci 119: 290–299, 2011

Key words: polyethylene nanocomposite; nonisothermal crystallizatin kinetics; aspect ratio; multiwall carbon nanotubes; activation energy; secondary crystallization

INTRODUCTION

The microstructure of the polymer and nanomaterials play an important role in determining the polymer nanocomposite mechanical, optical, rheological, and thermal properties. In this study, the influence of structure of carbon nanotubes (CNT) and its loading on the thermal properties of polyethylene/CNT nanocomposites is investigated. The study of polymer crystallization kinetics is significant from theoretical and practical points of view.[1–9] Many researchers have investigated the crystallization behavior of different polyethylenes.[10–15]

The previous research has primarily focused on the study of the influence of molecular weight (M_w), molecular weight distribution (MWD), branch type, branch content (BC), and crystallization conditions on the crystallization behavior of ethylene/α-olefin copolymers.[16–28] Most of these studies used Ziegler–Natta linear low density polyethylenes (ZN-LLDPEs). Due to the random comonomer composition and sequence distribution, and intermolecular heterogeneity of ZN-LLDPEs, the effects of the individual factors on the crystallization phenomenon are difficult to separate. For example, an increase in BC, a lamella first becomes shorter, then segmented, and eventually disintegrates into small crystallites.[28] Also, the previous studies used primarily fractions of conventional heterogeneous ZN-LLDPEs.[16,18,21,25,29]

Several studies on the thermal properties and molecular structure of metallocene LLDPE (m-LLDPEs) have been reported by different authors.[26,30,31–42] Most of these studies focused on the influence of short chain branch distribution[26,31–33,37,40–42] on melting and crystallization kinetics, particularly of a single polymer and its fractions using different fractionation techniques.[34,35,37–39] Bensason et al.[30] classified homogeneous ethylene/1-octene copolymers on the basis of comonomer content and reported the melting phenomena and crystal morphology by relating their results to the tensile and dynamic mechanical properties. Seo et al.[43]

Correspondence to: I. A. Hussein (ihussein@kfupm.edu.sa).

Contract grant sponsors: Center of Research Excellence in Petroleum Refining & Petrochemicals (CoRE-PRP, Ministry of Higher Education), KFUPM.

TABLE I
Elementary Compositions of MWCNT Used in this study

Components	Contents (%)
C	97.34
Cl	0.21
Fe	0.56
Ni	1.87
S	0.02

reinforced polypropylene (PP) with multiwalled carbon nanotubes (MWCNTs), varying the weight fraction from 1 to 5%. They studied the crystallization kinetics and evaluated the isothermal crystallization parameters (n and k) for Avrami. They deduced that the addition of 1% MWCNTs increases the crystallization rate by as much as an order of magnitude or higher and is attributed to enhanced nucleation, resulting from the presence of MWCNTs.

Funck and Kaminsky[44] produced PP/MWCNT composites by *in situ* polymerization. They studied the half time of crystallization for the produced composites using Avrami plots. They observed that crystallization rate increased with decreasing isothermal crystallization temperature and higher loadings with MWCNT for all materials that they investigated.

Vega et al.[45] produced nanocomposite samples by melt mixing a high density polyethylene (HDPE) with an *in situ* polymerized HDPE/MWCNT masterbatch. They also conclude that crystallization kinetics studied through Differential Scanning Calorimetery (DSC) suggest that the MWCNTs act as nucleating agents for polymeric chains. The length of the MWCNTs (short vs long) would likely affect the nucleation of polymeric chains. Therefore, we would like to investigate the effect of aspect ratio and chemical modification of CNT on the nonisothermal crystallization kinetics, which has not been reported in the literature. In this study, we will use LDPE and MWCNT to investigate these parameters. In addition, the effect of CNT loading will be studied.

EXPERIMENTAL

Materials and sample preparation

MWCNTs with different aspect ratios and surface modification were supplied by Cheap Tubes, USA. Table I shows energy dispersive X-ray spectroscopy data provided by the supplier. In Table II, details of the three different CNTs used in the study are given. The three different types are selected to study one parameter at a time. The long and the short CNTs have the same ID and OD; however, the length of the long CNT is 12 times greater than that of the short CNTs. The aspect ratio is defined as the ratio of length/OD. Therefore a comparison of the long and short MWCNT will reveal the impact of aspect ratio. On the other hand, a comparison of MWCNT and COOH-MWCNT will highlight the influence of chemical modification as both CNTs have the same ID, OD, and length.

In all of the MWCNT used, 95% percent of the total weight is MWCNT and approximately 1.5% of the weight was ash, and the rest was by products from MWCNT production. MWCNTs used were not washed or purified. As stated by the producing company, COOH-MWCNT contains 0.7% —COOH groups. The LDPE with a melt index of 0.75 g/10 min has a weight average molecular weight of 99.5 kg/mol and a MWD of 6.5 and a total short branch content of 22 branches/1000 C as determined by GPC and NMR, respectively, according to the literature reported by Hussein and Williams.[46] The LDPE resin and MWCNT-LDPE composites were conditioned (or blended) in a Haake PolyDrive melt blender. The blending temperature used was 190°C. The rpm was 50 and time of blending was 10 min. From here onwards the long, short, and COOH modified MWCNT will be named LCNT, SCNT, and MCNT, respectively.

Differential scanning Calorimetery

All measurements were performed using a TA Q1000 instrument equipped with a liquid nitrogen cooling system and auto sampler. Nitrogen at a flow rate 50 mL/min was used to purge the instrument to prevent degradation of the samples upon thermal treatments. The DSC was calibrated in terms of melting temperature and heat of fusion using a high purity indium standard (156.6°C and 28.45 J/g). The absolute crystallinity was calculated using the heat of fusion of a perfect polyethylene crystal, 290 J/g.[47]

Composite samples (7.5–10 mg) were sliced and compressed into a nonhermetic aluminum pans. To minimize the thermal lag between the sample and the pan, samples with flat surface were used. An empty aluminum pan was used as reference. The previous thermal effects were removed by heating the samples from room temperature to 140°C; followed by a hold up at 140°C for 5 min. All samples

TABLE II
Dimensions of the Multiwalled Carbon Nanotubes (MWCNT)

Name	OD[a] (nm)	ID[b] (nm)	Length (μm)	Aspect ratio (L/D)
Long MWCNT 95 wt %	30–50	5–15	10–20	375
Short MWCNT 95 wt %	30–50	5–15	0.5–2.0	31
COOH-MWCNT 95 wt %	30–50	5–15	10–20	375

[a] Outer diameter.
[b] Inner diameter.

were cooled to subambient temperatures for complete evaluation of crystallization.[25] The samples were cooled from 140° to 5°C at a rate of 2°C/min, 6°C/min, and 10°C/min. First, the baseline was calibrated using empty crimped aluminum pans. All testing was performed in the standard DSC mode.

THEORY AND CALCULATION

Nonisothermal crystallization kinetics

Several analytical methods have been developed to describe the nonisothermal crystallization kinetics of polymers: (1) modified Avrami analysis,[2,48–50] (2) Ozawa analysis,[2] (3) Ziabicki analysis,[51,52] and other methods.[53,54] In this study, the modified Avrami analysis proposed by Jeziorny[3] and the Mo method suggested by Liu et al.[55] were used to describe the nonisothermal crystallization kinetics of LDPE/MWCNT composites. Because of the variation in the range of crystallization temperatures, the Ozawa model[2] was not suitable for this study. The Avrami equation is defined as follows:[48–50]

$$1 - X_t = \exp(-k_t t^n) \tag{1}$$

where n is the Avrami crystallization exponent, which is dependent on the nucleation mechanism and growth dimensions; t is the crystallization time; k_t is the growth rate constant, which depends on nucleation and crystal growth; and X_t is the relative crystallinity.[50] X_t is defined as follows:

$$X_t = \frac{\int_{t_0}^{t} \left(\frac{dH_c}{dt}\right) dt}{\int_{t_0}^{t_\infty} \left(\frac{dH_c}{dt}\right) dt} \tag{2}$$

where dH_c/dt is the rate of heat evolution and t_0 and t_α are the onset and completion times of the crystallization process, respectively. The Avrami equation was developed on the basis of the assumption that the crystallization temperature is constant. Jeziorny[3] modified the equation to describe nonisothermal crystallization. At a chosen cooling rate (R), the relative crystallinity is a function of the crystallization temperature (T). That is, eq. (2) can be formulated as

$$X_T = \frac{\int_{T_0}^{T_c} \left(\frac{dH_c}{dT}\right) dT}{\int_{T_0}^{T_\infty} \left(\frac{dH_c}{dT}\right) dT} \tag{3}$$

where X_T is the relative crystallinity as a function of crystallization temperature, T_0 denotes the crystallization onset temperature, and T_c and T_∞ represent the crystallization temperatures at time t and after the completion of the crystallization process, respectively. Also, time t can be calculated from T_c using the following equation:[2,51]

$$t = \frac{T_0 - T}{R} \tag{4}$$

where R is the cooling rate (°C/min). The double-logarithmic form of eq. (1) yields

$$\ln[-\ln(1 - X_t)] = \ln k_t + n \ln t \tag{5}$$

Thus, n and the crystallization rate constant (k_t) can be obtained from the slope and intercept of the plot of ln[-ln(1-X_t)] versus ln t, respectively, for each R. The physical meaning of k_t and n cannot be related to the nonisothermal case in a simple way; they provide further insight into the kinetics of nonisothermal crystallization. The rate of nonisothermal crystallization depends on R. Therefore, k_t can be corrected to obtain the corresponding primary rate constant (k_R).[2]

$$\ln k_R = \frac{\ln k_t}{R} \tag{6}$$

A method modified by Mo, which combines the Avrami equation with the Ozawa equation, was also used to describe the nonisothermal crystallization. Its final form is given as follows:[55]

$$\ln R = \ln F(T) - \alpha \ln t \tag{7}$$

where Mo modified crystallization rate parameter $(F(T)) = [k(T)/k_t]^{1/m}$ represents the value of R and α is the ratio of n to the Ozawa exponent (m; $\alpha = n/m$).

Furthermore, the effective activation energy (ΔE_x) was calculated theoretically with the method proposed by Vyazovkin and Sbirrazzuoli.[56] In this method, the coefficient of the growth rate (G) and the overall crystallization rate (dX/dt) are related by

$$\frac{-E}{R} = \frac{d\ln G}{dT^{-1}} = \frac{d\ln\left(\frac{dX}{dt}\right)}{dT^{-1}} \tag{8}$$

G is given as a function of T_c by the Hoffman–Lauritzen equation in the context of the Hoffman–Lauritzen secondary nucleation theory.[57] Vyazovkin and Sbirrazzuoli[56] modified the Hoffman–Lauritzen equation to calculate ΔE_x at a given conversion (X) from the following relationship:

$$\Delta E_x = U^* \frac{T^2}{(T - T_\infty)^2} + K_g R \frac{(T_m^0)^2 - T^2 - T_m^0 T}{(T_m^0 - T)^2 T} \tag{9}$$

where U^* denotes the activation energy per segment, which characterizes the molecular diffusion across the interfacial boundary between melt and crystals; T_∞ is usually set equal to T_g-30 K, where T_g is the glass-transition temperature of the polymer; K_g is a nucleation constant; T_m^o is the equilibrium melting

point for the polymer, and R is the gas constant. The Vyazovkin and Sbirrazzuoli method and Hoffman–Lauritzen theory have been widely used in recent literature to calculate U^* and K_g.[58–61]

RESULTS AND DISCUSSION

The nonisothermal crystallization MDSC traces (nonreversing curves) of pure LDPE and its nanocomposites at low and high R values (2, 6, and 10°C/min) are shown in Figure 1(a–c). For all the samples with varying nanocomposite amount, the DSC thermograms showed no change in the baseline above 120°C and below 30°C. So, these values are used as the initial and final values for all of the DSC calculations, if applicable. The LDPE nanocomposites crystallization exotherms were fairly similar. They showed a distinct high temperature peak followed by a broad long tail. However, it can distinctly be observed from Figure 1(a–c) that as the amount of MWCNT in the composite is increased, early onset of crystallization takes place. For example, at the low cooling rate (2°C/min) T_{onset} increases from an average value of 105.38°C for 0.5 wt % MWCNT to 106.85°C for the 5.0 wt % MWCNT. However, the effect of both the aspect ratio and COOH modification at this low cooling rate is much less as given by the data shown in Table III. Table III was prepared using the TA analysis software. For each exotherm, the peak and onset crystallization were found using the software options. Similarly, the influence of aspect ratio or COOH modification on T_{peak} is weak.

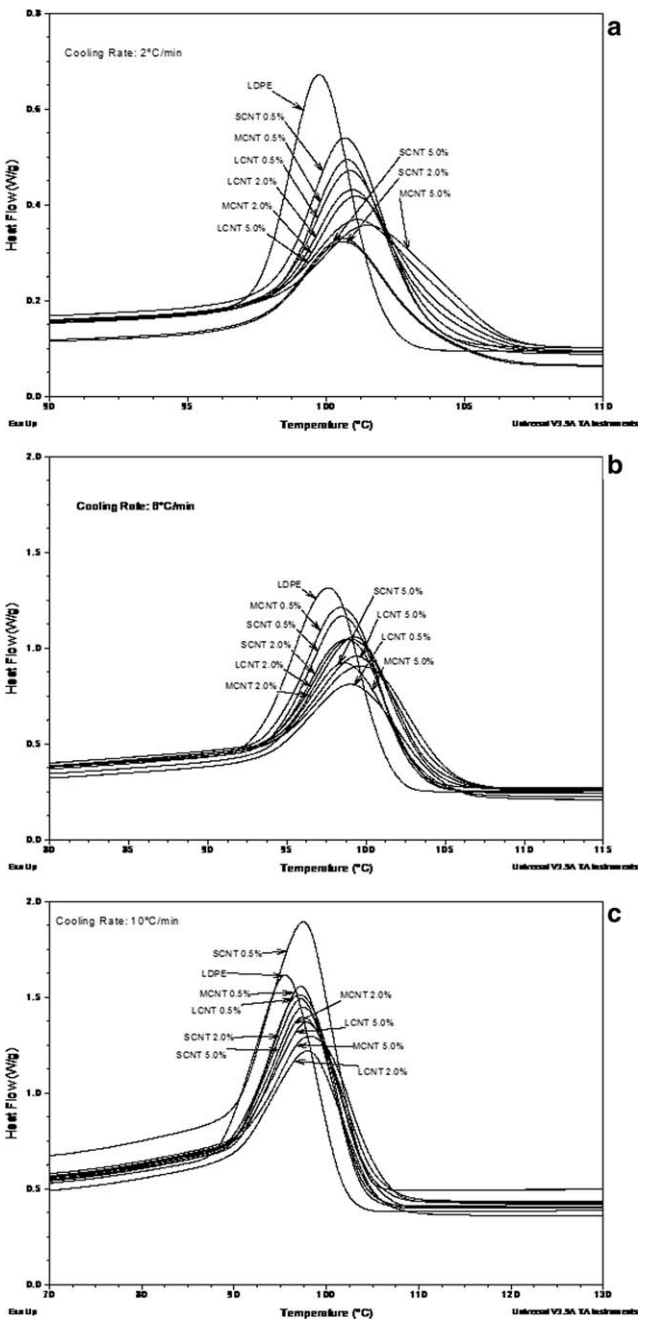

Figure 1 Nonisothermal crystallization exotherms of LDPE/MWCNT nanocomposites with R's of (a) 2, (b) 6, and (c) 10°C/min.

TABLE III
Peak and Onset Crystallization Temperatures for Different Nanocomposites

Cooling rate (°C/min)	Weight %	MWCNT type	T_{Peak} (°C)	T_{Onset} (°C)
2	0.5	Long	100.85	105.34
		Short	100.66	105.08
		Modified	100.75	105.71
	2.0	Long	100.95	105.84
		Short	100.61	106.21
		Modified	101.05	106.08
	5.0	Long	101.14	106.82
		Short	100.61	106.88
		Modified	101.50	106.86
10	0.5	Long	97.10	105.81
		Short	97.50	104.94
		Modified	97.2	104.64
	2.0	Long	97.95	107.10
		Short	97.25	105.12
		Modified	97.45	105.94
	5.0	Long	97.90	108.01
		Short	97.50	106.69
		Modified	98.2	107.12

At high cooling rate (10°C/min), LCNT showed higher T_{onset} values that increase with MWCNT concentration. A comparison of LCNT and MCNT (both have the same aspect ratio) and the LCNT and SCNT suggests that aspect ratio has influenced T_{onset} but not T_{peak} with weak influence of surface modification on T_{peak} as well as T_{onset}. This suggests that the effect of aspect ratio on T_{onset} is cooling rate dependent and it is more pronounced at high cooling rate. On the other hand, the impact of aspect ratio or surface modification of MWCNT on T_{peak} is very weak. This observation can be explained, tentatively,

TABLE IV
Percent Crystallinity of Various LDPE/MWCNT Nanocomposites

Cooling rate (°C/min)	Weight %	MWCNT type	Total crystallinity (%)
2	0.5	Long	39.97
		Short	37.54
		Modified	38.86
	2.0	Long	37.69
		Short	34.52
		Modified	37.68
	5.0	Long	36.97
		Short	31.16
		Modified	36.65

as follows: CNT with high aspect ratio (LCNT) promotes nucleation due to its large surface area per tube. However, for T_{peak} the surface area of CNT is no longer a factor in enhancing crystallization since crystallization is already at its peak. Therefore, the increase in MWCNT concentration shifts T_{onset} to higher values and promotes nucleation with almost no effect on T_{peak}. Nevertheless, we observed that at low cooling rates surface modification, and aspect ratio did not affect T_{onset} or T_{peak}. In general, there was a decrease in total crystallinity due to the addition of MWCNT, which is a direct result of the decrease of the polymer portion in the nanocomposite.

Further, we tried to assess the impact of aspect ratio and surface modification on the total crystallinity as it is an important property and it impacts mechanical properties. Table IV shows the percent crystallinity, X_{Total}, that was calculated using the Q1000 software. The initial point for the integration was chosen as 2°C above the onset temperature for each exotherm and the final point was room temperature. At low cooling rates (2°C/min) and for low concentrations (0.5%) there is no significant influence of surface modification or aspect ratio on total crystallinity. However, both LCNT and MCNT nanocomposites show higher values of X_{Total} in comparison with the SCNT. At such low concentrations, COOH modification is not influencing total crystallinity but aspect ratio is a factor with high aspect ratio yielding higher total crystallinity. The decrease in polymer total crystallinity due to the addition of CNT is obvious and is expected.

The relative crystallinity X_T was calculated using eq. (3) and shown in Figure 2(a–c) for the different cooling rates. X_T was then converted into X_t using eq. (4). X_t versus t is plotted in Figure 3(a–c). The whole data of LDPE nanocomposites was used to fit Avrami model but it is known that it will not fit the entire crystallization range [see Ref. [62] and references therein]. Avrami equation was used to fit data in the range of $X_T = 0$–40% crystallization. But we encountered the problem getting $n > 4$ which has no physical meaning.[53] Figure 4 represents sample Avrami plots for all LDPE nanocomposites obtained at 2°C/min. Avrami equation was used to fit data in the range of $X_T = 0$–40%. The rest of the results and extracted parameters are shown in Table V. Table VI shows the comparison of Avrami parameter and fit quality at 40 and 95% crystallinity. It is observed that if the whole data is fitted, the values of Avrami

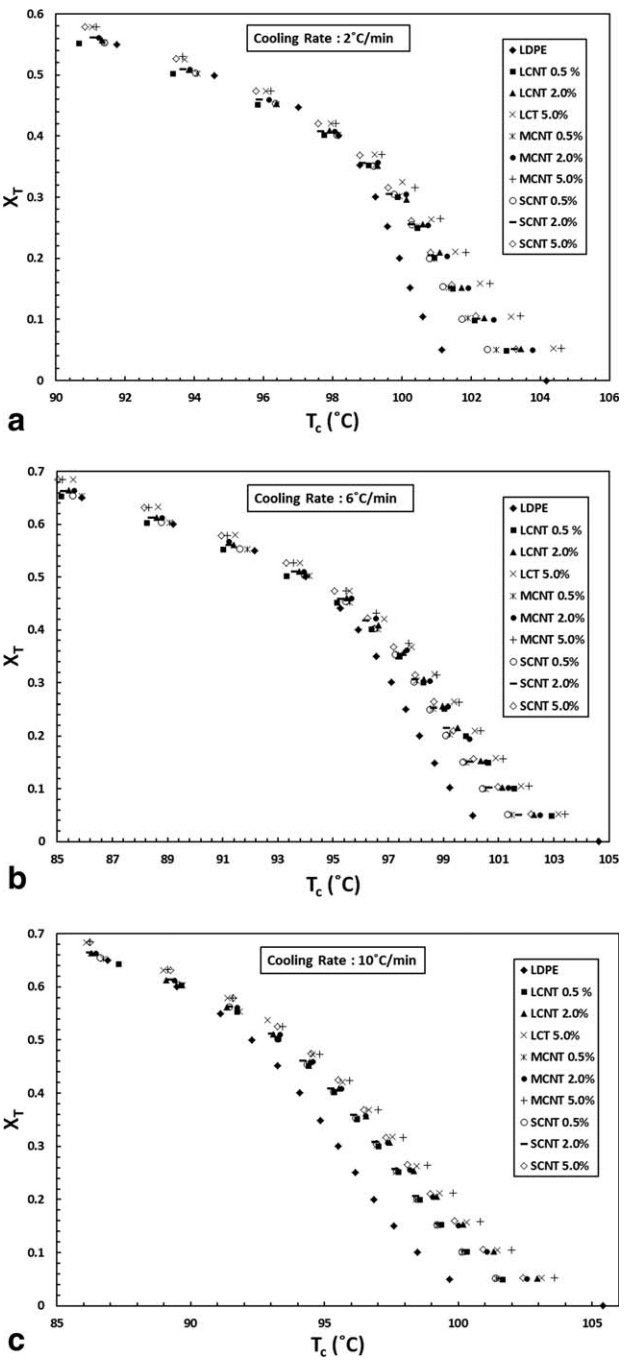

Figure 2 X_T vs. T_c for LDPE/MWCNT nanocomposites at different cooling rates: (a) 2, (b) 6, and (c) 10°C/min.

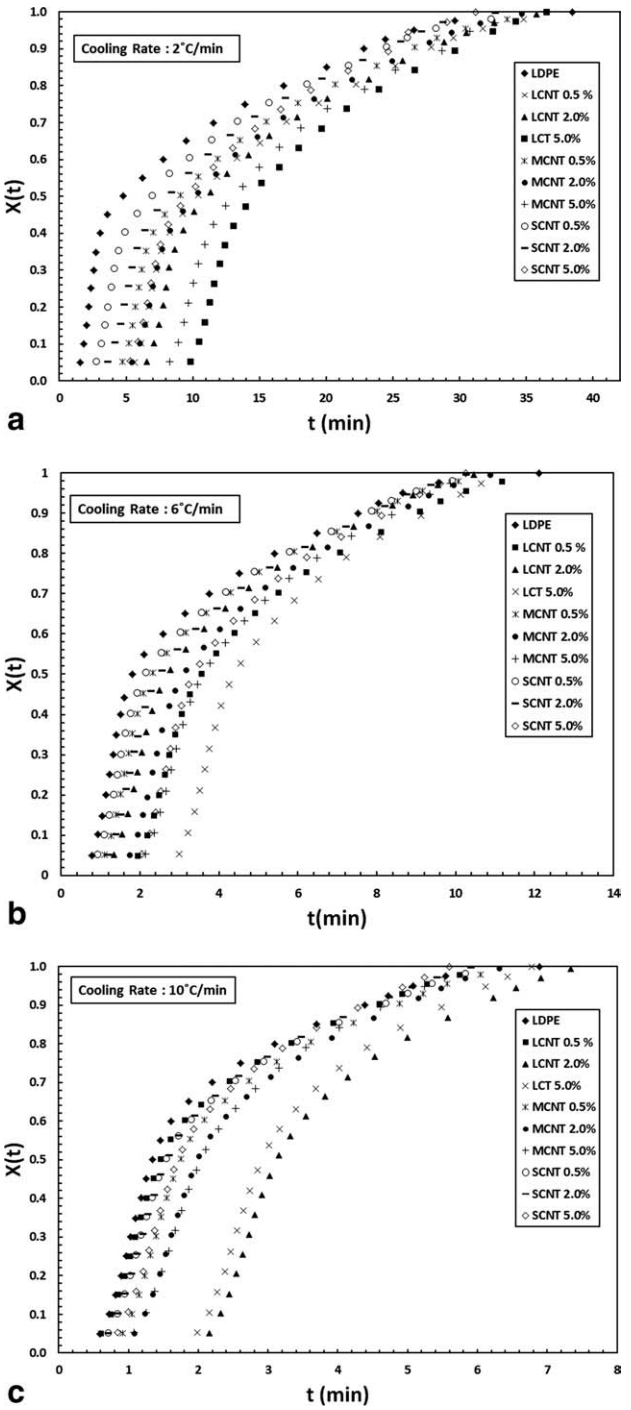

Figure 3 X_t vs t for LDPE/MWCNT nanocomposites at different cooling rates: (a) 2, (b) 6, and (c) 10°C/min.

parameter make sense but the data fit is very poor as reflected in the regression coefficient. But if selective fitting for upto 40% crystallization is done, the Avrami parameter loses its physical meaning. Hence, no attempt was made to discuss the results obtained by Avrami method in this paper.

The kinetic model proposed by Mo[55] was used [see eq. (7)]. Sample plots of ln R versus ln t for

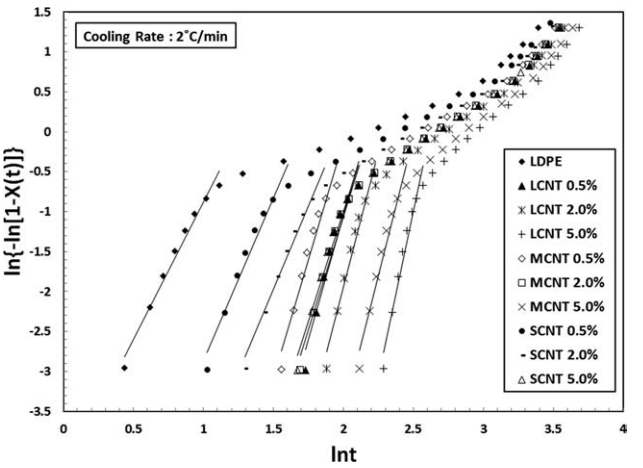

Figure 4 Avrami plot for LDPE/MWCNT nanocomposites obtained at 2°C/min.

LDPE nanocomposite with 5 wt % MWCNT are shown in Figure 5(a–c). Plots for the rest of nanocomposites are not shown here; however, the Mo parameters for all samples are given in Table VII. From these plots, values of α and $F(T)$ were obtained at different crystallinities in the range 20–80%. All plots were linear, as predicted by eq. (7). $F(T)$ increased with the increase in percentage crystallinity. In general, the higher the MWCNT loading, the higher the value of $F(T)$ for the same crystallinity. Also, for the same MWCNT loading $F(T)$ increases with crystallinity. This observation was valid at all levels of crystallization. These two observations suggest the increased difficulty of polymer

TABLE V
Avrami Parameters for LDPE/MWCNT Nanocomposites

Cooling rate (°C/min)	Sample	n_{40}	k_t	k_r	Regression coefficient (r^2)
2	LDPE	3.974	0.0094	0.0971	0.998
	LCNT 0.5%	8.299	3.1E-08	0.0001	0.997
	LCNT 2.0%	8.556	5.6E-09	7.49E-05	0.999
	LCNT 5.0%	9.255	4.26E-11	6.52E-06	0.984
	MCNT 0.5%	6.846	1.34E-06	0.001159	0.982
	MCNT 2.0%	6.992	3.77E-07	0.000614	0.999
	MCNT 5.0%	8.985	3.21E-10	1.79E-05	0.995
	SCNT 0.5%	4.625	0.000499	0.022348	0.984
	SCNT 2.0%	4.988	8.12E-05	0.009014	0.999
	SCNT 5.0%	6.619	8.65E-07	0.00093	0.996
10	LDPE	3.349	0.315373	0.89101	0.997
	LCNT 0.5%	3.143	0.315373	0.89101	0.997
	LCNT 2.0%	3.663	0.266602	0.876166	0.997
	LCNT 5.0%	6.853	0.000338	0.449734	0.974
	MCNT 0.5%	7.166	0.000444	0.462088	0.99
	MCNT 2.0%	4.749	0.081268	0.778022	0.998
	MCNT 5.0%	4.805	0.038504	0.722022	0.997
	SCNT 0.5%	4.916	0.036589	0.718349	0.999
	SCNT 2.0%	3.54	0.188624	0.846369	0.991
	SCNT 5.0%	3.772	0.191666	0.847724	0.999

TABLE VI
Avrami Parameters for LDPE/MWCNT Nanocomposites at 40 and 95% Crystallinity

Cooling rate (°C/min)	Sample	n_{40}	Regression coefficient (r^2)	n_{95}	Regression coefficient (r^2)
2	LDPE	3.974	0.998	1.063	0.903
	LCNT 0.5%	8.299	0.997	2.007	0.901
	LCNT 2.0%	8.556	0.999	1.977	0.897
	LCNT 5.0%	9.255	0.984	2.584	0.876
	MCNT 0.5%	6.846	0.982	1.632	0.887
	MCNT 2.0%	6.992	0.999	1.846	0.903
	MCNT 5.0%	8.985	0.995	2.355	0.886
	SCNT 0.5%	4.625	0.984	1.341	0.907
	SCNT 2.0%	4.988	0.999	1.596	0.921
	SCNT 5.0%	6.619	0.996	2.007	0.901
	Sample	n	r^2	n	r^2
10	LDPE	3.143	0.997	1.572	0.911
	LCNT 0.5%	3.663	0.997	1.595	0.93
	LCNT 2.0%	6.853	0.974	2.893	0.896
	LCNT 5.0%	7.166	0.99	3.02	0.908
	MCNT 0.5%	4.749	0.998	1.834	0.904
	MCNT 2.0%	4.805	0.997	2.059	0.92
	MCNT 5.0%	4.916	0.999	2.194	0.924
	SCNT 0.5%	3.54	0.991	1.675	0.917
	SCNT 2.0%	3.772	0.999	1.758	0.932
	SCNT 5.0%	4.053	0.999	1.999	0.934

crystallization at high crystallinity and with the addition of CNT. The results of Mo method of analysis are in agreement with the previous Avrami analysis where k_r was observed to decrease with increasing MWCNT loading. So, MWCNT promotes initial crystallization but at the expense of slower secondary crystallization process.

The Vyazovkin and Sbirrazzuoli[56] method of analysis [eq. (9)], which is based on Hoffman–Lauritzen theory for secondary crystallization,[57] was used for the analysis of the activation energy data. Temperature is plotted against Activation energy for 30–75% relative crystallinity of the nanocomposites. We can clearly observe in Figure 6(a) that the activation energy is decreasing as the amount of MWCNT is increased in the bulk from 0.5% to 5.0% weight. This suggests that the incorporation of CNT promotes the initial crystallization process by lowering the activation energy. In Figure 6(b), Temperature is plotted against activation energy for different kinds of MWCNT at a fixed loading of 5 wt %. In general, the presence of MWCNT resulted in significant reduction in activation energy for long, short, and modified MWCNT. Also, both LCNT and MCNT (both have same aspect ratio) showed similar reduction in activation energy over the whole temperature range. Nevertheless, the long CNT resulted in more drop in activation energy in comparison with short CNT. This suggests that CNT with long aspect ratio are enhancing the crystallization process as compared to CNT with short aspect ratio. However, for the same long aspect ratio the —COOH modification did not result in a reduction of the activation energy. These results are in agreement with findings from previous methods of analysis.

A model was proposed for fitting the above activation energy; crystallization temperature and

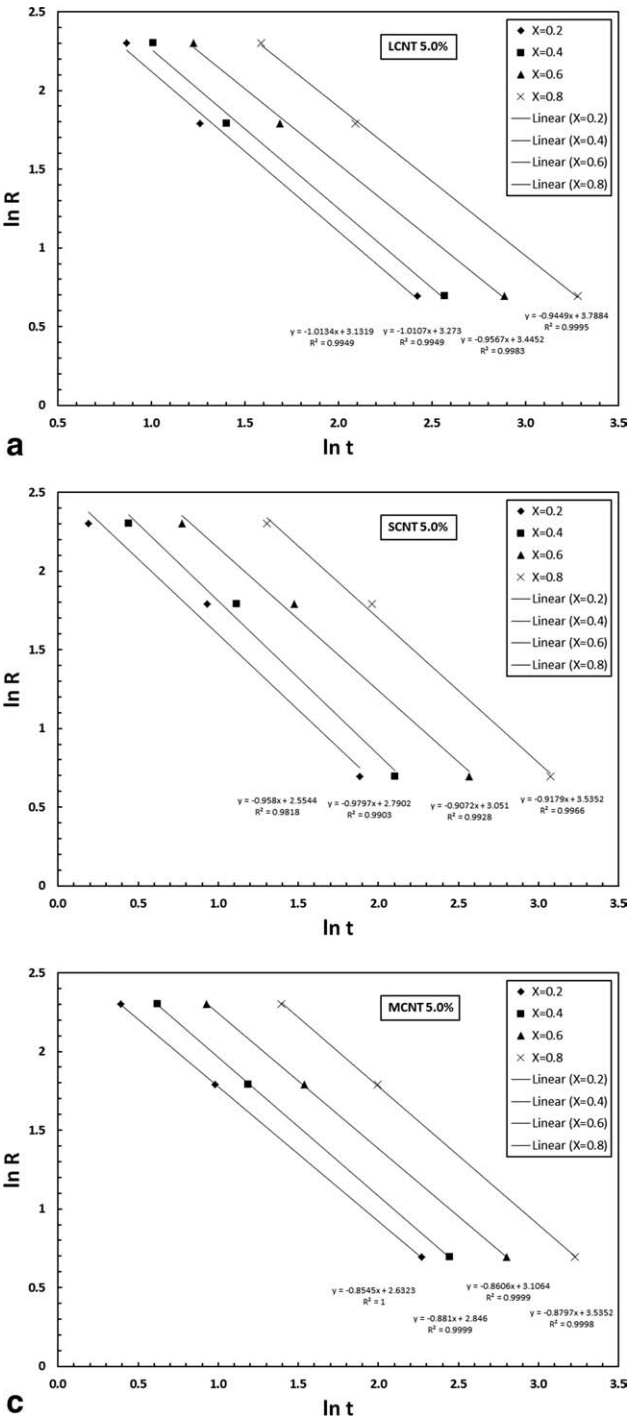

Figure 5 Plots of ln R versus ln t at each given relative crystallization: (a) LCNT 5.0%, (b) SCNT 5.0%, and (c) MCNT 5.0%.

TABLE VII
Values of the Mo Parameters, α and *F*(*T*), at a Fixed Value of the Relative Degree of Crystallinity [*X*(*t*)] for All of the LDPE/Nanocomposites

		X(*t*)%			
Sample	Variable	20	40	60	80
LDPE	α	1.749	1.661	1.019	0.952
	F(*T*)	2.069	2.531	2.777	3.387
	r^2	0.997	0.996	0.999	0.999
LCNT 0.5	α	0.817	0.859	0.813	0.856
	F(*T*)	2.342	2.585	2.858	3.382
	r^2	0.959	0.97	0.979	0.992
LCNT 2.0	α	0.938	0.98	0.988	0.982
	F(*T*)	2.719	2.948	3.31	3.757
	r^2	0.742	0.793	0.912	0.972
LCNT 5.0	α	1.013	1.01	0.956	0.944
	F(*T*)	3.131	3.273	3.445	3.788
	r^2	0.994	0.994	0.998	0.999
MCNT 0.5	α	0.968	0.989	0.903	0.913
	F(*T*)	2.358	2.6	2.909	3.452
	r^2	0.961	0.968	0.992	0.998
MCNT 2.0	α	1.033	1.036	0.941	0.933
	F(*T*)	2.644	2.874	3.114	3.574
	r^2	0.997	0.998	0.999	1
MCNT 5.0	α	0.854	0.881	0.86	0.879
	F(*T*)	2.632	2.846	3.106	3.535
	r^2	1	0.999	0.999	0.999
SCNT 0.5	α	1.217	1.184	0.974	0.95
	F(*T*)	2.251	2.568	2.904	3.468
	r^2	0.985	0.986	0.998	1
SCNT 2.0	α	1.039	1.029	0.923	0.93
	F(*T*)	2.34	2.607	2.923	3.471
	r^2	0.999	0.999	1	0.999
SCNT 5.0	α	0.958	0.979	0.907	0.917
	F(*T*)	2.554	2.79	3.051	3.535
	r^2	0.981	0.99	0.992	0.996

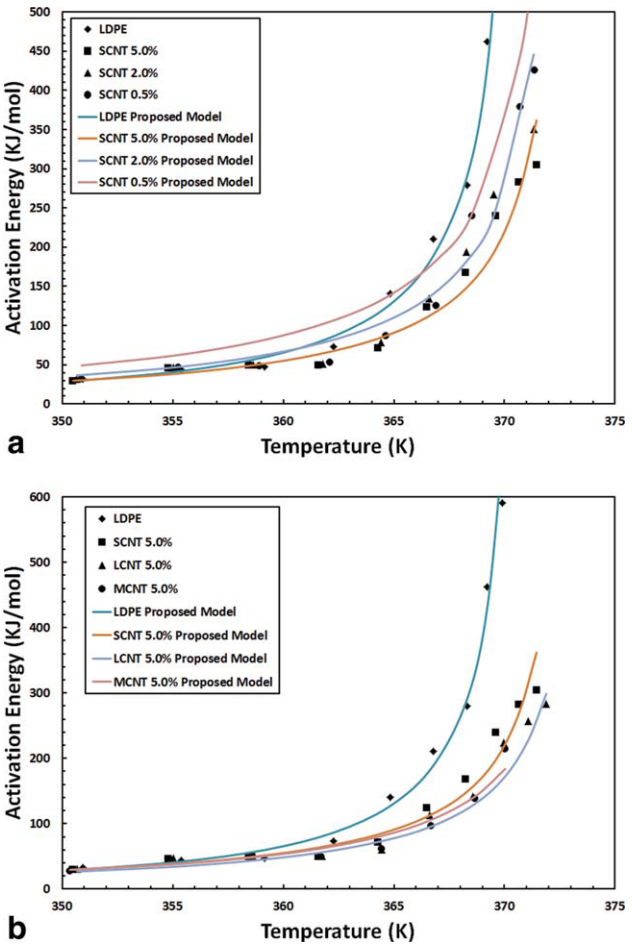

Figure 6 Plots of the activation energy versus crystallization temperature for (a) LDPE/varying loading of SCNT, (b) LDPE with different MWCNT at 5 wt %. Continuous lines show predictions of the proposed model. [Color figure can be viewed in the online issue, which is available at wileyonlinelibrary.com.]

relative crystallinity. The proposed model is given below:

$$E = ae^{-bX_tT} \tag{10}$$

where E is the activation energy, a and b are constants. X_t is relative crystallinity and T is absolute temperature. After linearization of the above equation ln E was plotted against X_tT to obtain a straight line. A very good fit was obtained. Model parameters are given in Table VIII. It was observed that constant b is almost independent of concentration. In fact b was in the range 0.15 to 0.18. Therefore an average value of 0.165 was used for fitting the whole data. Therefore constant b is unique and reflects the specific crystallization process. Further, the value of b is almost the same for long, short or modified MWCNT at the same MWCNT concentration. However, the constant a is concentration dependent and it decreases with increasing concentration. Therefore, the activation energy function is separable into two terms: a concentration dependent term (constant a) and a temperature dependent term (exponential term).

Figure 7(a,b) show the SEM results for SCNT nanocomposite with 5 wt % loading. The figures clearly show that there is agglomeration of the SCNT within the matrix but these agglomerations are well distributed in the matrix. A similar trend was observed for LCNT and MCNT and at different loadings. As all nanocomposites under investigation

TABLE VIII
Parameter Values for the Proposed Model

	a	*b*	Regression coefficient (r^2)
LDPE	1283	0.023	0.986
MCNT, 5.0	2008	0.016	0.940
LCNT, 5.0	1815	0.015	0.959
SCNT, 5.0	2273	0.016	0.966
SCNT, 2.0	2813	0.017	0.960
SCNT, 0.5	3782	0.018	0.970

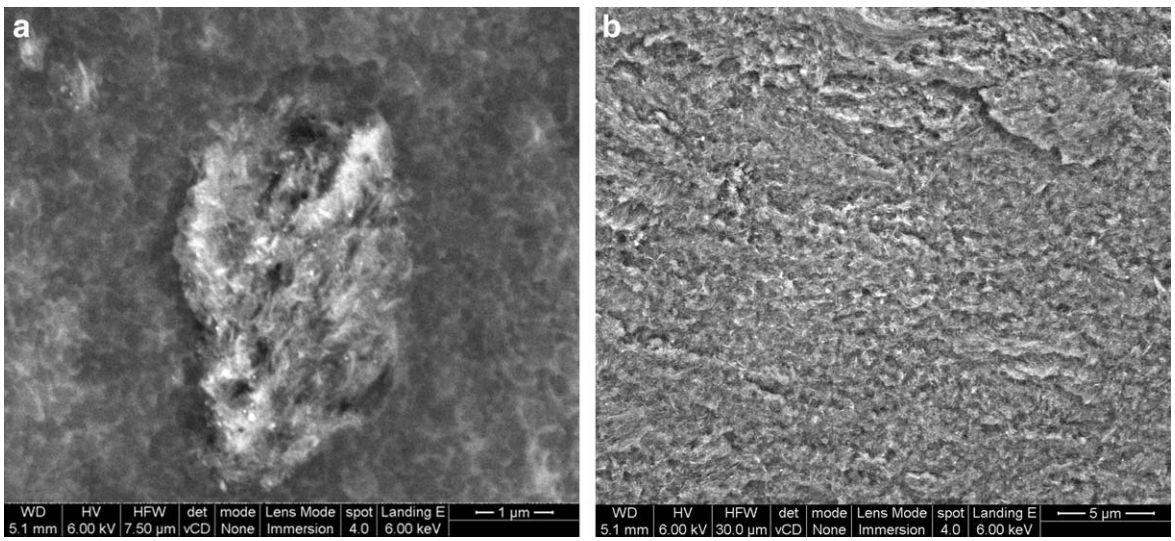

Figure 7 SEM results for SCNT nanocomposite with 5 wt % loading (a) high magnification (b) low magnification.

showed the same agglomeration, no attempt is made to relate the results with degree of dispersion.

CONCLUSION

In this article, the effect of CNT loading surface modification and aspect ratio was studied. The presence of long MWCNT promotes initial crystallization and it impacts both the onset as well as peak crystallization temperatures. The effect is more pronounced at high cooling rates. Also, —COOH modified MWCNT behaved in a very similar fashion like unmodified MWCNT with the same length. On the other hand, the increased MWCNT loading helps in initiating the crystallization process but it slows the secondary crystallization. The surface modification with short group such as —COOH did not make any noticeable difference on the crystallization process. Three different methods of data analyses were used: The Avrami approach, Mo method, and Hoffman-Lauritzen theory. However, nothing was deduced from the Avrami method. The other two methods agree that the addition of MWCNT promoted the initial crystallization by shifting the onset crystallization temperature to higher values. However, the crystallization process is slowed after that. For example with increasing MWCNT concentration, long crystallization tails following the peak crystallization temperature were obtained. On the other hand, $F(T)$ obtained from Mo model increased with the increase in MWCNT concentration and percent crystallinity indicating the increased difficulty in crystallization. Further, the Hoffman-Lauritzen theory showed that the activation energy decreased with the increase in MWCNT concentration which supports the observed promotion of the initial crystallization. A model was proposed to correlate the effect of MWCNT concentration, crystallization temperature, and crystallinity on the activation energy ($E = ae^{-0.165X_iT}$). The model was able to fit the whole set of data obtained at different cooling rates and for short and long MWCNT.

References

1. Evans, U. R. Trans Faraday Soc 1945, 41, 365.
2. Ozawa, T. Polymer 1971, 12, 150.
3. Jeziorny, A. Polymer 1978, 19, 1142.
4. Hay, J. N.; Mills, P. J. Polymer 1982, 23, 1380.
5. McHugh, A. J.; Burghardt, W. R.; Holland, D. A. Polymer 1986, 27, 1585.
6. Jayakannan, M.; Ramakrishnan, S. J Appl Polym Sci 1999, 74, 59.
7. Parasnis, N. C.; Ramani, K. J Therm Anal Calorim 1999, 55, 709.
8. Sajkiewicz, P.; Carpaneto, L.; Wasiak, A. Polymer 2001, 42, 5365.
9. Qiu, Z.; Ikehara, T.; Nishi, T. Polymer 2003, 44, 5429.
10. Kao, Y. H.; Phillips, P. J. Polymer 1986, 27, 1669.
11. Phillips, P. J.; Kao, Y. H. Polymer 1986, 27, 1679.
12. Nordmeier, E.; Lanver, U.; Lechner, M. D. Macromolecules 1990, 23, 1072.
13. Sutton, S. J.; Vaughan, A. S.; Bassett, D. C. Polymer 1996, 37, 5735.
14. Wagner, J.; Abu-Iqyas, S.; Monar, K.; Phillips, P. J. Polymer 1999, 40, 4717.
15. Wagner, J.; Phillips, P. J. Polymer 2001, 42, 8999.
16. Mandelkern, L.; Maxfield, J. J Polym Sci Polym Phys Ed 1979, 17, 1913.
17. Strobl, G. R.; Engelke, T.; Maderek, E.; Urban, G. Polymer 1983, 24, 1585.
18. Maderek, E.; Strobl, G. R. Colloid Polym Sci 1983, 261, 471.
19. Alamo, R.; Domszy, R.; Mandelkern, L. J Phys Chem 1984, 88, 6587.
20. Mandelkern, L. Polym J 1985, 17, 337.
21. Usami, T.; Gotoh, Y.; Takayama, S. Macromolecules 1986, 19, 2722.
22. Alamo, R. G.; Mandelkern, L. Macromolecules 1989, 22, 1273.
23. Fatou, J. G.; Marco, C.; Mandelkern, L. Polymer 1990, 31, 1685.
24. Alamo, R. G.; Viers, B. D.; Mandelkern, L. Macromolecules 1993, 26, 5740.

25. Shanks, R. A.; Amarasinghe, G. J Therm Anal Calorim 2000, 59, 471.
26. Zhang, M.; Lynch, D. T.; Wanke, S. E. Polymer 2001, 42, 3067.
27. Rabiej, S.; Goderis, B.; Janicki, J.; Mathot, V. B. F.; Koch, M. H. J.; Groeninckx, G.; Reynaers, H.; Gelan, J.; Wlochowicz, A. Polymer 2004, 45, 8761.
28. Jiao, C.; Wang, Z.; Liang, X.; Hu, Y. Polym Test 2004, 24, 71.
29. Voigt-Martin, I. G.; Alamo, R.; Mandelkern, L. J Polym Sci Part B: Polym Phys 1986, 24, 1283.
30. Bensason, S.; Minick, J.; Moet, A.; Chum, S.; Hiltner, A.; Baer, E. J Polym Sci Part B: Polym Phys 1996, 34, 1301.
31. Keating, M. Y.; Lee, I. H. J Macromol Sci Phys 1999, 38, 379.
32. Starck, P.; Lehmus, P.; Seppala, J. V. Polym Eng Sci 1999, 39, 1444.
33. Xu, J.; Xu, X.; Feng, L. Eur Polym J 1999, 36, 685.
34. Janimak, J. J.; Stevens, G. C. Thermochim Acta 1990, 332, 125.
35. Razavi-Nouri, M.; Hay, J. N. Polymer 2001, 42, 8621.
36. Fu, Q.; Chiu, F. C.; He, T.; Liu, J.; Hsieh, E. T. Macromol Chem Phys 2001, 202, 927.
37. Wang, C.; Chu, M. C.; Lin, T. L.; Lai, S. M.; Shih, H. H.; Yang, J. C. Polymer 2000, 42, 1733.
38. Chiu, F. C.; Fu, Q.; Peng, Y.; Shih, H. H. J Polym Sci Part B: Polym Phys 2002, 40, 325.
39. Starck, P.; Lofgren, B. Eur Polym J 2002, 38, 97.
40. Teng, H.; Shi, Y.; Jin., X. J Polym Sci Part B: Polym Phys 2002, 40, 2107.
41. Hussein, I. A. Polym Int 2004, 53, 1327.
42. Islam, M. A.; Hussein, I. A.; Atiqullah, M. Eur Polym J 2007, 43, 599.
43. Seo, M. K.; Lee, J. R.; Park, S. J. Mater Sci Eng A 2005, 404, 79.
44. Funck, A.; Kaminsky, W. Compos Sci Technol 2007, 67, 906.
45. Vega, J. F.; Martinez-Salazar, J.; Trujillo, M.; Arnal, M. L.; Muller, A. J.; Berdeau, S.; Dubios, Ph. Macromolecules 2009, 42, 4719.
46. Hussein, I. A.; Williams, M. C. Macromolecules 2000, 33, 520.
47. Turi, E. A. Ed. Thermal Characterization of Polymeric Materials, 2nd Ed.; Academic Press: New York, 1997; vol 1.
48. Avrami, M. J Chem Phys 1939, 7, 1103.
49. Avrami, M. J Chem Phys 1940, 8, 212.
50. Avrami, M. J Chem Phys 1941, 9, 177.
51. Ziabbicki, A. Appl Polym Symp 1967, 6, 1.
52. Ziabbicki, A. Colloid Polym Sci 1974, 252, 433.
53. Wunderlich, B. Macromolecular Physics; Academic Press: New York, 1976; Vol. 2.
54. Tanem, B. S.; Stori, A. Polymer 2001, 42, 5389.
55. Liu, T.; Mo, Z.; Wang, S.; Zhang, H. Polym Eng Sci 1997, 37, 568.
56. Vyazovkin, S.; Sbirrazzuoli, N. Macromol Rapid Commun 2004, 25, 733.
57. Hoffman, J. D.; Davis, G. T.; Lauritzen, J. I. Jr.; Hannay, N. B., Eds. Treatise on Solid State Chemistry, Plenum: New York, 1976; Vol. 3.
58. Achilias, D. S.; Papageorgiou, G. Z.; Karayannidis, G. P. Macromol Chem Phys 2005, 206, 1511.
59. Cai, J.; Li, T.; Han, Y.; Zhuang, Y.; Zhang, X. J Appl Polym Sci 2006, 100, 1479.
60. Vyazovkin, S.; Dranca, I. Macromol Chem Phys 2006, 207, 20.
61. Botines, E.; Puiggali, J. Eur Polym J 2006, 42, 1595.
62. Hussein, I. A. J Appl Polym Sci 2008, 107, 2802.